

Folding model study of the isobaric analog excitation: isovector density dependence, Lane potential and nuclear symmetry energy

Dao T. Khoa,* Hoang Sy Than, and Do Cong Cuong

Institute for Nuclear Science & Technique, VAEC,

P.O. Box 5T-160, Nghia Do, Hanoi, Vietnam.

(Dated: June 8, 2007; accepted for publication in Phys. Rev. C)

Abstract

A consistent folding model analysis of the ($\Delta S = 0, \Delta T = 1$) charge exchange (p, n) reaction measured with ^{48}Ca , ^{90}Zr , ^{120}Sn and ^{208}Pb targets at the proton energies of 35 and 45 MeV is done within a two-channel coupling formalism. The nuclear ground state densities given by the Hartree-Fock-Bogoljubov formalism and the density dependent CDM3Y6 interaction were used as inputs for the folding calculation of the nucleon optical potential and (p, n) form factor. To have an accurate isospin dependence of the interaction, a complex isovector density dependence of the CDM3Y6 interaction has been carefully calibrated against the microscopic Brueckner-Hartree-Fock calculation by Jeukenne, Lejeune and Mahaux before being used as folding input. Since the isovector coupling was used to explicitly link the isovector part of the nucleon optical potential to the cross section of (p, n) reaction exciting the 0^+ isobaric analog states in ^{48}Sc , ^{90}Nb , ^{120}Sb and ^{208}Bi , the newly parameterized isovector density dependence could be well tested in the folding model analysis of the (p, n) reaction. The isospin- and density dependent CDM3Y6 interaction was further used in the Hartree-Fock calculation of asymmetric nuclear matter, and a realistic estimation of the nuclear symmetry energy has been made.

PACS numbers: 24.50.+g, 25.60.Bx, 25.60.Lg,

*Electronic address: khoa@vaec.gov.vn

I. INTRODUCTION

The charge exchange (p, n) reaction is well known as an effective tool to excite the isobaric analog of the target ground state. Such an isobaric analog state (IAS) has essentially the same structure as the ground state of the target except for the replacement of a neutron by a proton and, hence, differs in energy approximately by the Coulomb energy of the added proton. In the isospin representation, the two states are just two members of the isospin multiplet which differ only in the orientation of the isospin \mathbf{T} . The similarity of the initial and final states of the (p, n) reaction makes this reaction very much like an elastic scattering in which the isospin of the incident proton is “flipped”. Indeed, the isospin dependent part of the proton-nucleus optical potential (OP) was used by Satchler *et al.* [1] some 40 years ago as the charge exchange form factor in their study of the (p, n) reaction within the distorted wave Born approximation (DWBA). In general, the central nucleon-nucleus OP can be written in terms of the isovector coupling [2] as

$$U(R) = U_0(R) + 4U_1(R)\frac{\mathbf{t}\cdot\mathbf{T}}{A}, \quad (1)$$

where \mathbf{t} is the isospin of the incident nucleon and \mathbf{T} is that of the target A . The second term of Eq. (1), known as the Lane potential, contributes to the elastic (p, p) and (n, n) scattering as well as to the charge exchange (p, n) reaction [3]. While the relative contribution by the Lane potential U_1 to the elastic nucleon scattering cross section is small and amounts only a few percent for a neutron-rich target [4, 5], it determines entirely the (Fermi-type) $\Delta J^\pi = 0^+$ transition strength of the (p, n) reaction to isobaric analog states. Therefore, the (p, n) reaction can be used as a reliable probe of the isospin dependence of the proton-nucleus OP.

The nucleon-nucleus OP has been studied over the years and there are several “global” sets of the OP parameters deduced from the extensive optical model analyses of nucleon elastic scattering, like that by Becchetti and Greenlees [6], the CH89 global OP [7], and a recent systematics by Koning and Delaroche [8] which covers a wide range of energies (from 1 keV to 200 MeV) and target masses ($24 \leq A \leq 209$). Although parameterized in the empirical Woods-Saxon form, these global systematics are very valuable in predicting the nucleon-nucleus OP when elastic scattering data are not available or cannot be measured which is the case for the unstable, dripline nuclei. Given a large neutron excess in the unstable neutron-rich nuclei, it is important to know as accurate as possible the isospin

dependence of the nucleon-nucleus OP before using it in various studies of nuclear reactions and nuclear astrophysics. We recall here the two main methods used so far to determine the isospin dependence of the nucleon-nucleus OP:

(i) study the elastic scattering of proton and neutron from the same target and measured at about the same energy, where the isovector term of Eq. (1) has the same strength, but opposite signs for (p, p) and (n, n) elastic scattering;

(ii) study the (isospin-flip) charge exchange (p, n) transition between isobaric analog states.

Since there are not sufficient high-quality (p, n) data available for a wide range of target masses and proton energies, the empirical isospin dependence of the nucleon-nucleus OP has been deduced [6, 7, 8] based mainly on method (i). While these three global nucleon optical potentials have been widely used in predicting the nucleon-nucleus OP in numerous direct reaction analyses within the DWBA or coupled-channel (CC) formalism, their isospin dependence has been rarely used to study the charge exchange (p, n) transition between the IAS's. The (phenomenological) Lane potential U_1 has been studied in details so far at some particular energies only, like the systematics for U_1 deduced from IAS data of the (p, n) reaction measured at 22.8 [9] and 35 MeV [10]. Therefore, it is necessary to have a reliable microscopic prediction for U_1 by the folding model, to reduce the uncertainty associated with the isospin dependence of the nucleon-nucleus OP.

Another very interesting microscopic aspect of the Lane potential is that it provides a direct link between the isospin dependence of the in-medium nucleon-nucleon (NN) interaction and the charge exchange (p, n) reaction, so that accurately measured (p, n) cross section can serve as a good probe of the isospin dependence of the NN interaction [11] if the wave functions of the involved nuclear states are known. Furthermore, within the frame of many-body calculation of nuclear matter (NM), the asymmetry of the NM equation of state (EOS) depends entirely on the density- and isospin dependence of the NN interaction [12, 13]. This asymmetry is actually determined by the NM symmetry energy $S(\rho)$ which is defined in terms of the NM binding energy $B(\rho, \delta)$ as

$$B(\rho, \delta) = B(\rho, 0) + S(\rho)\delta^2 + O(\delta^4) + \dots \quad (2)$$

where $\delta = (\rho_n - \rho_p)/\rho$ is the neutron-proton asymmetry parameter. The contribution of $O(\delta^4)$ and higher-order terms in Eq. (2), i.e., the deviation from the parabolic law was proven

to be negligible [12, 13]. The knowledge about the nuclear EOS (2) is well known to be vital for the understanding of the dynamics of supernova explosion and neutron star formation [14, 15, 16]. The NM symmetry energy determined at the saturation density, $E_{\text{sym}} = S(\rho_0)$ with $\rho_0 \approx 0.17 \text{ fm}^{-3}$, is widely known in the literature as the *symmetry energy* or symmetry coefficient. Although numerous nuclear many-body calculations have predicted E_{sym} to be around 30 MeV [12, 13, 17, 18], a direct experimental determination of E_{sym} still remains a challenging task. One needs, therefore, to relate E_{sym} to some experimentally inferrable quantity like the neutron skin in neutron-rich nuclei [19, 20, 21, 22] or fragmentation data of the heavy-ion (HI) collisions involving $N \neq Z$ nuclei [23, 24, 25]. In our recent study of the IAS excitation in the $p(^6\text{He}, ^6\text{Li}^*)n$ reaction using the folded Lane potential U_1 for the charge exchange form factor [26], we have shown how the NM symmetry energy can be linked to the charge exchange (p, n) transition strength and, hence, be probed in the folding model analysis of the (p, n) reaction. To extend the folding model study of the (p, n) reaction to heavier targets to validate the conclusion made in Ref. [26] for the NM symmetry energy, we have studied in the present work the quasi-elastic (p, n) scattering measured by the MSU group for ^{48}Ca , ^{90}Zr , ^{120}Sn , and ^{208}Pb targets at the incident proton energies of 35 and 45 MeV [11]. For a detailed probe of the isospin dependence of the in-medium NN interaction, a (complex) isospin- and density dependence of the CDM3Y6 interaction [27] has been carefully parameterized based on the Brueckner-Hatree-Fock (BHF) calculation of nuclear matter by Jeukenne, Lejeune and Mahaux [28]. While the isovector part of the nucleon-nucleus OP in the NM limit has been investigated in numerous BHF studies (see, e.g., Ref. [29] and references therein), the isospin dependence predicted by such BHF calculations was rarely tested in the DWBA or CC analysis of the charge exchange reaction to isobaric analog states. Our present folding model study provides, therefore, an important method to link the BHF results to the descriptions of the quasi-elastic (p, n) reaction. By using the Lane potential U_1 to construct the charge exchange (p, n) form factor based on the isospin coupling, it is also straightforward to probe the isospin dependence of existing global nucleon-nucleus OP [6, 7, 8]. In the present work, the description of the considered (p, n) reactions by the three global nucleon optical potentials [6, 7, 8] has been given, with a detailed comparison between the results given by the CH89 potential [7] and those of the folding model analysis.

II. IAS EXCITATION, LANE POTENTIAL AND ISOSPIN COUPLING

A. General formalism

We give here a brief introduction to the coupled-channel formalism for the charge exchange (p, n) reaction to isobar analog states, and interested readers are referred to Ref. [3] for more technical details. Let us restrict our consideration to a given isospin multiplet with fixed values of isospin \mathbf{t} for the projectile and \mathbf{T} for the target. Then, the isospin projections are $T_z = (N - Z)/2$ and $\tilde{T}_z = T_z - 1$ for the target nucleus A and *isobaric analog nucleus* \tilde{A} , respectively. We further denote, in the isospin representation, state formed by adding a proton to A as $|pA\rangle$ and adding a neutron to \tilde{A} as $|n\tilde{A}\rangle$. The transition matrix elements of the isovector part of the nucleon-nucleus optical potential (1) can then be obtained [3] for the elastic nucleon-nucleus scattering as

$$\langle \tau A | 4U_1(R) \frac{\mathbf{t} \cdot \mathbf{T}}{A} | \tau A \rangle = \pm \frac{2}{A} T_z U_1(R), \text{ with } \tau = p, n. \quad (3)$$

The $+$ sign in the right-hand side of Eq. (3) pertains to incident neutron and $-$ sign to incident proton. Similarly, the transition matrix element or (p, n) form factor (FF) for the $(\Delta T = 1)$ charge exchange $A_{\text{g.s.}}(p, n)\tilde{A}_{\text{IAS}}$ reaction is obtained as

$$\langle n\tilde{A} | 4U_1(R) \frac{\mathbf{t} \cdot \mathbf{T}}{A} | pA \rangle \equiv F_{pn}(R) = \frac{2}{A} \sqrt{2T_z} U_1(R). \quad (4)$$

In the two-channel approximation for the charge exchange (p, n) reaction to IAS, the total wave function is written as

$$\Psi = |pA\rangle \chi_{pA}(\mathbf{R}) + |n\tilde{A}\rangle \chi_{n\tilde{A}}(\mathbf{R}), \quad (5)$$

where the waves $\chi(\mathbf{R})$ describe the relative motion of the scattering system. Then, the elastic (p, p) scattering and charge exchange $A_{\text{g.s.}}(p, n)\tilde{A}_{\text{IAS}}$ cross sections can be obtained from the solutions of the following coupled-channel equations [3]

$$[K_p + U_p(R) - E_p] \chi_{pA}(\mathbf{R}) = -F_{pn}(R) \chi_{n\tilde{A}}(\mathbf{R}), \quad (6)$$

$$[K_n + U_n(R) - E_n] \chi_{n\tilde{A}}(\mathbf{R}) = -F_{pn}(R) \chi_{pA}(\mathbf{R}). \quad (7)$$

Here $K_{p(n)}$ and $E_{p(n)}$ are the kinetic-energy operators and center-of-mass energies of the $p + A$ and $n + \tilde{A}$ partitions. The OP in the entrance $(p + A)$ and outgoing $(n + \tilde{A})$ channels

are determined explicitly through the isoscalar (U_0) and isovector (U_1) parts of the nucleon optical potential (1) as

$$U_p(R) = U_0(R) - \frac{2}{A}T_z U_1(R), \quad (8)$$

$$U_n(R) = U_0(R) + \frac{2}{A}(T_z - 1)U_1(R). \quad (9)$$

In the CC calculation, both U_p and U_n are added by the corresponding spin-orbital potential as well as U_p added by the Coulomb potential of the $p+A$ system. Since the energies of isobar analog states are separated approximately by the Coulomb displacement energy, the (p, n) transition between them has a nonzero Q value. To account for this effect, the isoscalar U_0 and isovector U_1 potentials used to construct $F_{pn}(R)$ and $U_n(R)$ are evaluated at an effective incident energy of $E = E_{\text{lab}} - Q/2$, midway between the energies of the incident proton and emergent neutron, as suggested by Satchler *et al.* [1].

Since the existing global OP parameters [6, 7, 8] can be used to construct the isoscalar and isovector components of the proton-nucleus OP at the considered energies, it is straightforward to test those parameters in the description of the $A_{\text{g.s.}}(p, n)\tilde{A}_{\text{IAS}}$ reaction to isobaric analog states. However, more interesting structure information can be obtained when $U_{0(1)}$ are evaluated microscopically using an appropriate folding approach [4].

B. Folding model

In our version [4, 5] of the single-folding model, the central nucleon-nucleus potential V is evaluated as a Hartree-Fock-type potential

$$V = \sum_{j \in A} [\langle ij | v_D | ij \rangle + \langle ij | v_{\text{EX}} | ji \rangle], \quad (10)$$

where v_D and v_{EX} are the direct and exchange parts of the effective NN interaction between the incident nucleon i and nucleon j bound in the target A . The antisymmetrization of the nucleon-nucleus system is done by taking into account the knock-on exchange effects. To separate the isovector part of V which gives rise to the Lane potential, one needs to make explicit the isospin degrees of freedom. Namely, the following spin-isospin decomposition of the (energy- and density dependent) NN interaction is used

$$\begin{aligned} v_{\text{D(EX)}}(E, \rho, s) = & v_{00}^{\text{D(EX)}}(E, \rho, s) + v_{10}^{\text{D(EX)}}(E, \rho, s)(\boldsymbol{\sigma}\boldsymbol{\sigma}') \\ & + v_{01}^{\text{D(EX)}}(E, \rho, s)(\boldsymbol{\tau}\boldsymbol{\tau}') + v_{11}^{\text{D(EX)}}(E, \rho, s)(\boldsymbol{\sigma}\boldsymbol{\sigma}')(\boldsymbol{\tau}\boldsymbol{\tau}'), \end{aligned} \quad (11)$$

where s is the internucleon distance and ρ is the nuclear density around the interacting nucleon pair. The contribution from the spin dependent terms (v_{10} and v_{11}) in Eq. (11) to the central nucleon-nucleus potential (10) is exactly zero for a spin-saturated target like those considered in the present work.

Using the explicit proton (ρ_p) and neutron (ρ_n) densities in the folding input, the nucleon-nucleus potential (10) can be obtained [4] in terms of the isoscalar (V_{IS}) and isovector (V_{IV}) parts as

$$V(E, \mathbf{R}) = V_{\text{IS}}(E, \mathbf{R}) \pm V_{\text{IV}}(E, \mathbf{R}), \quad (12)$$

where the $+$ sign pertains to incident neutron and $-$ sign to incident proton. Each term in Eq. (12) consists of the corresponding direct and exchange potentials

$$V_{\text{IS}}(E, \mathbf{R}) = \int \{ [\rho_n(\mathbf{r}) + \rho_p(\mathbf{r})] v_{00}^{\text{D}}(E, \rho, s) + [\rho_n(\mathbf{R}, \mathbf{r}) + \rho_p(\mathbf{R}, \mathbf{r})] v_{00}^{\text{EX}}(E, \rho, s) j_0(k(E, R)s) \} d^3r, \quad (13)$$

$$V_{\text{IV}}(E, \mathbf{R}) = \int \{ [\rho_n(\mathbf{r}) - \rho_p(\mathbf{r})] v_{01}^{\text{D}}(E, \rho, s) + [\rho_n(\mathbf{R}, \mathbf{r}) - \rho_p(\mathbf{R}, \mathbf{r})] v_{01}^{\text{EX}}(E, \rho, s) j_0(k(E, R)s) \} d^3r, \quad (14)$$

where $\rho(\mathbf{r}, \mathbf{r}')$ is one-body density matrix of the target nucleus with $\rho(\mathbf{r}) \equiv \rho(\mathbf{r}, \mathbf{r})$, $j_0(x)$ is the zero-order spherical Bessel function, and the local momentum of relative motion $k(E, R)$ is determined from

$$k^2(E, R) = \frac{2\mu}{\hbar^2} [E_{\text{c.m.}} - V(R) - V_{\text{C}}(R)]. \quad (15)$$

Here, μ is the nucleon reduced mass, $V(R)$ and $V_{\text{C}}(R)$ are, respectively, the central nuclear and Coulomb potentials in the entrance channel ($V_{\text{C}} \equiv 0$ for the neutron-nucleus system). More details of the folding calculation of V_{IS} and V_{IV} can be found in Ref. [4].

We have further used in the folding calculation the density dependent CDM3Y6 interaction [27] which is based on the original M3Y interaction deduced from the G-matrix elements of the Paris NN potential [30]. The density dependence of the *isoscalar* part of the CDM3Y6 interaction was introduced earlier in Ref. [27] and its parameters have been carefully tested in numerous folding model analyses [27, 32] of the elastic, refractive nucleus-nucleus and α -nucleus scattering. Since the *isovector* part of the interaction can be probed in a folding model analysis of the charge exchange reaction only, we have developed in the present work an accurate procedure to parameterize the isovector density dependence of the CDM3Y6

interaction based on the BHF results for the energy and density dependent nucleon OP in nuclear matter by Jeukenne, Lejeune and Mahaux (JLM) [28]. The details of the new treatment of the isovector density dependence of the CDM3Y6 interaction are discussed in Sec. IV below.

Given the isovector folded potential (14) determined entirely by the neutron-proton difference in the nuclear densities, it is necessary to have the nuclear densities determined as accurate as possible for a good prediction of the Lane potential. In the present work we have used for the considered targets the microscopic ground-state densities given by the Hartree-Fock-Bogoljubov approach [33] where the single particle basis includes also the continuum states. All the results of the optical model (OM) analysis of elastic nucleon-nucleus scattering and CC calculation of the $A_{\text{g.s.}}(p, n)\tilde{A}_{\text{IAS}}$ reaction have been obtained with the CC code ECIS97 written by Raynal [34].

III. PREDICTION BY THE GLOBAL OPTICAL POTENTIAL

To study the (p, n) reaction based on CC equations (6)-(7), one needs to determine the nucleon OP in the entrance (U_p) and outgoing (U_n) channels as accurate as possible. Since the elastic neutron scattering on a target being in its *excited* IAS cannot be measured (most of IAS's are either a short-lived bound state or an unbound resonance), we have determined U_n from the isoscalar U_0 and isovector U_1 parts of the proton-nucleus OP evaluated at the effective incident energy $E = E_{\text{lab}} - Q/2$, using Eq. (9). The existing nucleon-nucleus global OP's [6, 7, 8] have been carefully determined based on large experimental databases of both the elastic nucleon-nucleus scattering and analyzing power angular distributions, and it is natural to use them to construct U_p for our study. The OM description of the elastic proton scattering from ^{48}Ca , ^{90}Zr , ^{120}Sn , and ^{208}Pb targets at incident proton energy of 40 MeV given by the three global proton-nucleus OP's are shown in Fig. 1 together with the measured data [40, 41]. Except some underestimation of the calculated elastic cross section in $p+^{48}\text{Ca}$ case, the overall OM description of the considered elastic scattering data is reasonable. It should be noted that the isovector strength of the nucleon-nucleus OP is only about 2-3% of the total OP and its contribution to the elastic scattering cross section is too weak to allow us to probe the isospin dependence of the OP directly in the OM analysis of elastic scattering. Therefore, in a "Lane consistent" approach, the only probe of isospin dependence

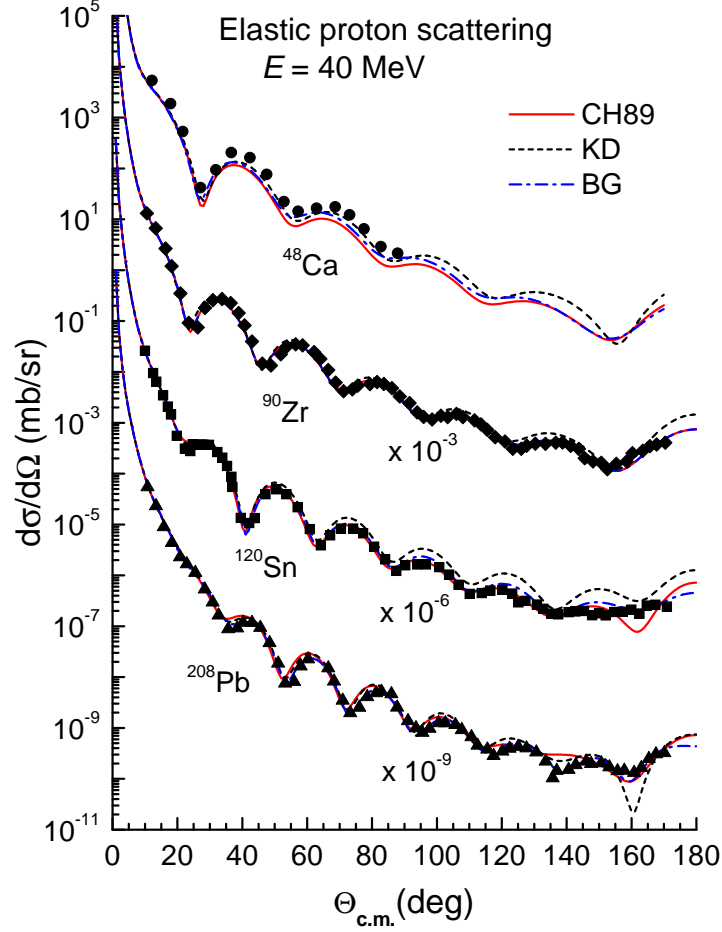


FIG. 1: (Color online) OM description of the elastic proton scattering from ^{48}Ca , ^{90}Zr , ^{120}Sn , and ^{208}Pb targets at 40 MeV obtained with the global OP by Becheetti and Greenlees (BG) [6], by Varner *et al.* (CH89) [7], and by Koning and Delaroche (KD) [8]. The data were taken from Refs. [40, 41].

of the nucleon-nucleus OP is the charge exchange $A_{\text{g.s.}}(p, n)\tilde{A}_{\text{IAS}}$ reaction to IAS. In such a quasi-elastic scattering, the charge exchange form factor (4) used in the CC equations (6)-(7) is determined entirely by the Lane potential U_1 . As a result, any variation of the U_1 strength and shape can sizably affect the calculated (p, n) cross section. Although all the three global OP's give about the same OM description of the elastic proton scattering as shown in Fig. 1, their descriptions of the charge exchange $A_{\text{g.s.}}(p, n)\tilde{A}_{\text{IAS}}$ reaction are quite different (see Figs. 2 and 3).

As discussed above, the isospin dependence of the nucleon global OP [6, 7, 8] has been

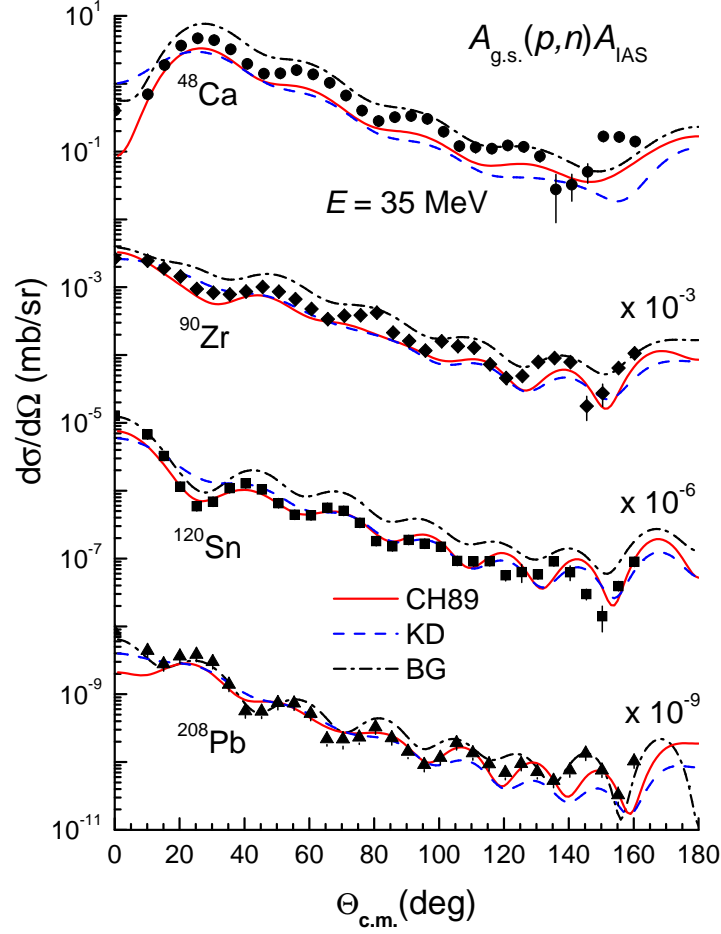


FIG. 2: (Color online) CC description of the charge exchange $A_{\text{g.s.}}(p,n)\tilde{A}_{\text{IAS}}$ reaction measured with ^{48}Ca , ^{90}Zr , ^{120}Sn , and ^{208}Pb targets at 35 MeV obtained with U_1 deduced from the global OP by Becheetti and Greenlees (BG) [6], by Varner *et al.* (CH89) [7], and by Koning and Delaroche (KD) [8]. The data were taken from Ref. [11].

determined from systematic OM studies of the elastic scattering of proton and neutron from the same target (at about the same energy), without any link to the $A_{\text{g.s.}}(p,n)\tilde{A}_{\text{IAS}}$ reaction. Given the absolute (p,n) cross section at least one order of magnitude weaker than the elastic (p,p) cross section, some discrepancy in the CC description of the (p,n) reaction using the Lane FF seen in Figs. 2-3 is not unexpected. From the three global OP's, U_1 determined from the systematics by Becheetti and Greenlees (BG) [6] is energy independent, and we found it too strong for the strength of the charge exchange form factor (4), especially, at energy of 45 MeV. Such a deficiency of the BG parameters for U_1 was

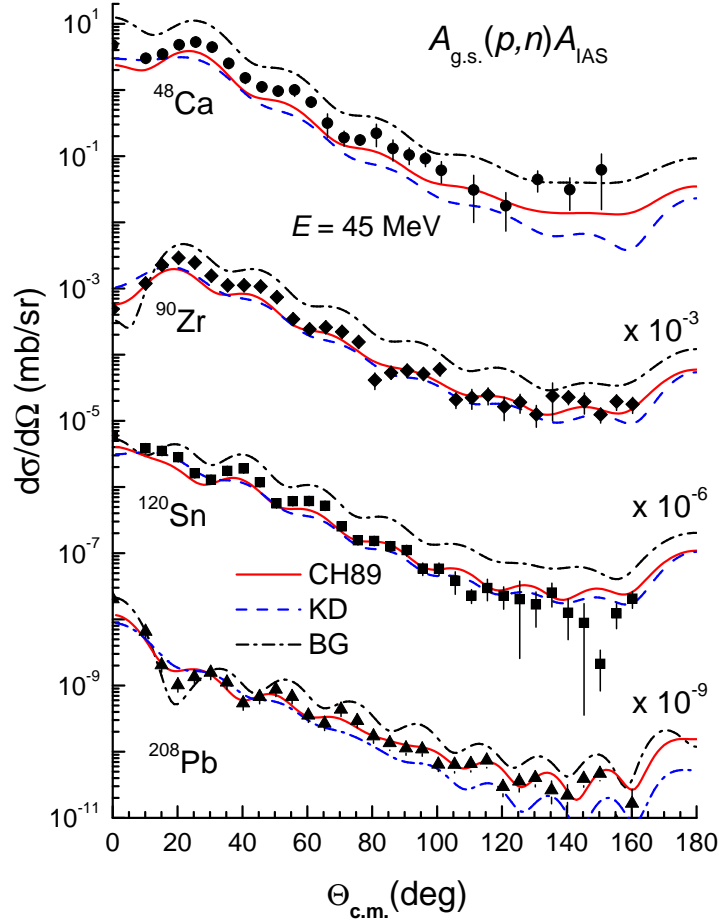


FIG. 3: (Color online) the same as Fig. 2 but for the (p, n) data measured at the proton energy of 45 MeV.

also found in the extensive OM analysis of elastic nucleon-nucleus scattering [7, 8]. The isovector parts of both the global optical potentials by Varner *et al.* (CH89) [7], and by Koning and Delaroche (KD) [8] were found to be energy dependent and weaker than that given by the BG systematics. Although the KD global OP is more recent and covers a much wider range of energies and target masses, from the CC results shown in Figs. 2-3 one can see that the description of $A_{g.s.}(p, n)\tilde{A}_{IAS}$ reaction by the KD global OP is slightly worse than that given by the CH89 global OP. A plausible reason is that the CH89 systematics was developed [7] with less constraints, based only on the elastic scattering data for $A \approx 40 - 209$ and energies of 16 to 65 MeV (for proton) and 10 to 26 MeV (for neutron). Although this range of energies and target masses is narrower than that covered by the KD global systematics [8], it includes the proton-nucleus systems considered in the present work. In

general, the Lane form factor (4) determined from the CH89 global OP gives a reasonable description of the $A_{\text{g.s.}}(p, n)\tilde{A}_{\text{IAS}}$ cross sections measured for ^{120}Sn and ^{208}Pb targets, and slightly underestimates the data for ^{48}Ca and ^{90}Zr targets. As will be shown below, such a suppression of the calculated $A_{\text{g.s.}}(p, n)\tilde{A}_{\text{IAS}}$ cross sections for the two lighter targets is due mainly to an enhanced absorption given by the CH89 global OP.

IV. FOLDING MODEL ANALYSIS

A. Isovector density dependence of the CDM3Y6 interaction

While the isoscalar density dependence of the CDM3Y6 interaction has been well tested in the folding model analysis [27, 32] of the elastic, refractive α -nucleus and nucleus-nucleus scattering, its *isovector* density dependence can be probed in the study of the charge exchange reaction only. In a recent work in this direction [26], we have used the same functional form for both the isoscalar and isovector density dependences and then fine tuned the scaling factor of the isovector part to fit the calculated (p, n) cross section to the data. Although we could reach good description of the (p, n) reaction under study [26], it remains desirable to have a more accurate assumption for the isovector density dependence based on the microscopic many-body calculation of nuclear matter. Therefore, we have developed in the present work a compact method to construct the isovector density dependence of the CDM3Y6 interaction based essentially on the BHF description of the nucleon OP in nuclear matter by Jeukenne, Lejeune and Mahaux [28]. We recall that the isoscalar density dependence of the CDM3Y6 interaction was introduced [27] as

$$v_{00}^{\text{D(EX)}}(E, \rho, s) = g(E)F_{\text{IS}}(\rho)v_{00}^{\text{D(EX)}}(s), \quad (16)$$

$$F_{\text{IS}}(\rho) = C_0[1 + \alpha_0 \exp(-\beta_0\rho) - \gamma_0\rho]. \quad (17)$$

Parameters of the isoscalar density dependence $F_{\text{IS}}(\rho)$ were chosen [27] to reproduce the NM saturation properties, with a nuclear incompressibility $K \approx 252$ MeV, in the Hartree-Fock (HF) calculation of symmetric NM. These parameters as well as those corresponding to other K values can be found in a recent review on the nucleus-nucleus potential [42]. The ‘intrinsic’ energy dependence of the isoscalar interaction is contained in the linear factor $g(E) \approx 1 - 0.0026E$, where E is the energy of incident nucleon. Given the success of the

TABLE I: Yukawa strengths of the central components of the M3Y-Paris interaction (19).

ν	R_ν (fm ⁻¹)	$Y_{00}^D(\nu)$ (MeV)	$Y_{01}^D(\nu)$ (MeV)	$Y_{00}^{\text{EX}}(\nu)$ (MeV)	$Y_{01}^{\text{EX}}(\nu)$ (MeV)
1	4.0	11061.625	313.625	-1524.25	-4118.0
2	2.5	-2537.5	223.5	-518.75	1054.75
3	0.7072	0.0	0.0	-7.8474	2.6157

parametrization (16)-(17) in numerous folding calculations, we have assumed in the present work a similar form for the isovector density dependence of the CDM3Y6 interaction

$$v_{01}^{\text{D(EX)}}(E, \rho, s) = F_{\text{IV}}(E, \rho) v_{01}^{\text{D(EX)}}(s). \quad (18)$$

The radial shapes of the isoscalar and isovector interactions were kept unchanged, as derived [12] from the M3Y-Paris interaction [30], in terms of three Yukawas

$$v_{00(01)}^{\text{D(EX)}}(s) = \sum_{\nu=1}^3 Y_{00(01)}^{\text{D(EX)}}(\nu) \frac{\exp(-R_\nu s)}{R_\nu s}. \quad (19)$$

One can see from the Yukawa strengths tabulated in Table I that the exchange terms Y_{01}^{EX} of the isovector interaction are much stronger than the direct terms Y_{01}^D (which is due to a cancellation between the even- and odd-state components). Therefore, an accurate evaluation of the exchange part of the isovector potential (14) is very essential in the folding model analysis of the (p, n) reaction. Such a domination of the exchange term in the isovector interaction has been first noted by Love [31]. In our folding approach [4] the exchange parts of both the isoscalar (13) and isovector (14) proton-nucleus potentials are evaluated using the *finite-range* exchange interaction $v_{00(01)}^{\text{EX}}(s)$ and are, therefore, more accurate than those given by a zero-range approximation for the exchange term.

Since the nucleon OP in nuclear matter can be defined [35, 36] as the *antisymmetrized* matrix elements of the effective NN interaction between the incident nucleon and those bound in the Fermi sea, it is given by the same Hartree-Fock-type potential (10), but using *plane waves* for the single-nucleon states [37, 38]. To determine the isovector density dependence, we have further adjusted the nucleon OP obtained with the CDM3Y6 interaction (in the NM limit) to reproduce the JLM density- and isospin dependent nucleon OP [28]. Since the JLM potential is *complex*, we have used two different CDM3Y functionals to match

separately the *real* and *imaginary* parts of the isovector CDM3Y6 potential to those of the JLM potential. Namely,

$$F_{\text{IV}}^u(E, \rho) = C_1^u(E)[1 + \alpha_1^u(E) \exp(-\beta_1^u(E)\rho) - \gamma_1^u(E)\rho], \quad (20)$$

so that the real ($u = V$) and imaginary ($u = W$) parts of the isovector CDM3Y6 interaction are determined as

$$v_{01}^{\text{D(EX)}}(E, \rho, s) = F_{\text{IV}}^V(E, \rho)v_{01}^{\text{D(EX)}}(s), \quad (21)$$

$$w_{01}^{\text{D(EX)}}(E, \rho, s) = F_{\text{IV}}^W(E, \rho)v_{01}^{\text{D(EX)}}(s). \quad (22)$$

Using Eq. (21), the isovector part of the *real* nucleon OP in the NM limit is given explicitly

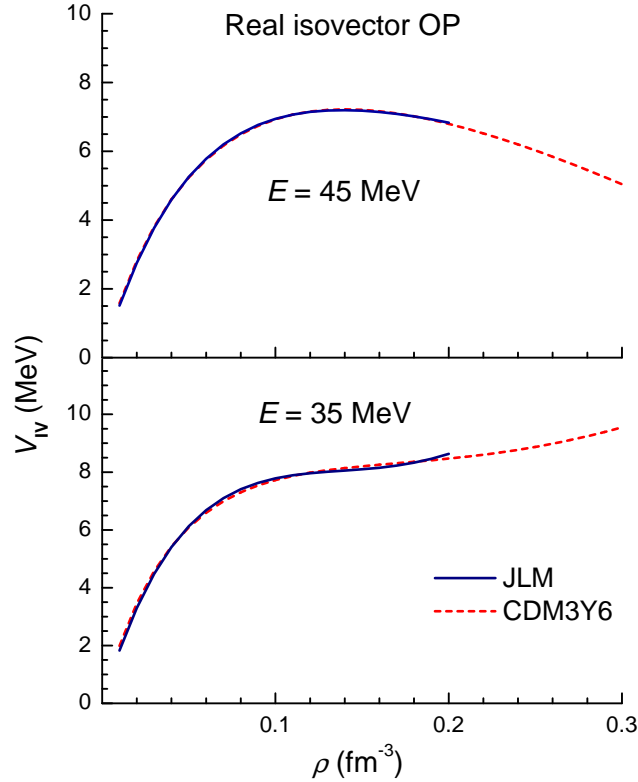


FIG. 4: (Color online) real part $V_{\text{IV}}(E, \rho)$ of the isovector nucleon OP given by the isovector density dependence (20) of the CDM3Y6 interaction in comparison with the JLM results [28] at $E = 35$ and 45 MeV.

as

$$V_{\text{IV}}(E, \rho) = F_{\text{IV}}^V(E, \rho) \{ (\rho_n - \rho_p) J_{01}^{\text{D}} + \int [\rho_n \hat{j}_1(k_F^n r) - \rho_p \hat{j}_1(k_F^p r)] v_{01}^{\text{EX}}(r) j_0(kr) d^3r \}. \quad (23)$$

Here $J_{01}^D = \int v_{01}^D(r) d^3r$, $\hat{j}_1(x) = 3j_1(x)/x$ and $j_1(x)$ is the first-order spherical Bessel function; ρ_n and ρ_p are the neutron and proton densities of asymmetric NM with a total density $\rho = \rho_n + \rho_p$ and the corresponding Fermi momenta $k_F^{p(n)} = (3\pi^2\rho_{p(n)})^{1/3}$. The momentum k of the incident nucleon of mass m is determined self-consistently [37] from the nucleon incident energy E and real OP as

$$k = \sqrt{\frac{2m}{\hbar^2} \{E - [V_{\text{IS}}(E, \rho) \pm V_{\text{IV}}(E, \rho)]\}}. \quad (24)$$

Here $V_{\text{IS}}(E, \rho)$ is the isoscalar part of the *real* nucleon OP, the (+) sign pertains to incident neutron and (-) sign to incident proton. Due to the self-consistent definition (24) of the momentum k , the isovector potential (23) is obtained by an iterative procedure. After $V_{\text{IV}}(E, \rho)$ is determined, the isovector part $W_{\text{IV}}(E, \rho)$ of the *imaginary* nucleon OP is obtained from the same Eq. (23), but with $F_{\text{IV}}^V(E, \rho)$ replaced by $F_{\text{IV}}^W(E, \rho)$. Our approach is to find re-

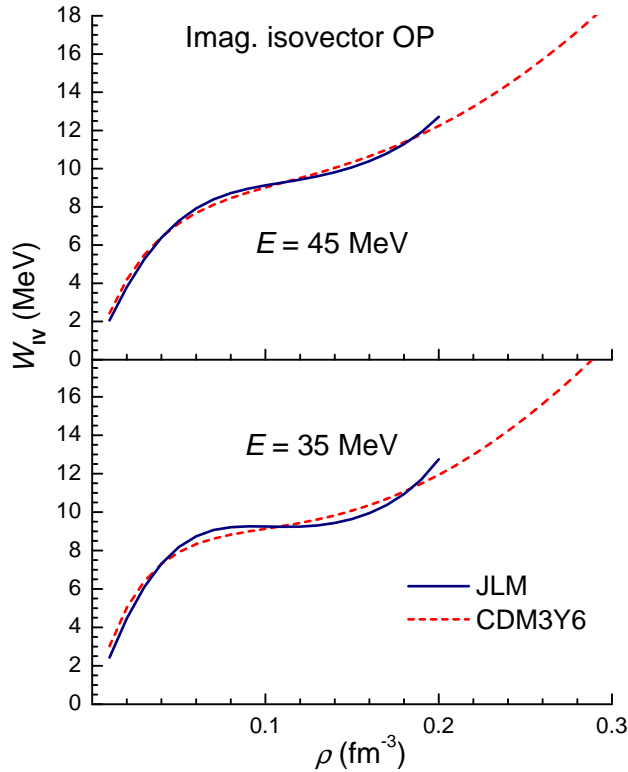


FIG. 5: (Color online) the same as Fig. 4 but for the imaginary part $W_{\text{IV}}(E, \rho)$ of the isovector nucleon OP.

alistic parameters of the isovector density dependence (20) of the CDM3Y6 interaction by

a χ^2 -fitting procedure which gives the isovector part of the nucleon OP as close as possible to that of the JLM nucleon optical potential $V_{\text{IV}}^{\text{JLM}}(E, \rho)$ tabulated in Ref. [28]. To keep a good accuracy of this fitting procedure, instead of introducing an energy dependent scaling factor like $g(E)$ in Eq. (16), the density dependent parameters in Eq. (20) have been adjusted separately at each energy. As illustration, the real $V_{\text{IV}}(E, \rho)$ and imaginary $W_{\text{IV}}(E, \rho)$ parts of the isovector nucleon OP at 35 and 45 MeV given by the best-fit density dependent parameters (20) are compared with the JLM results [28] in Figs. 4 and 5, respectively. For each target nucleus, the parameters of complex isovector density dependence have been searched individually at the effective incident energy $E = E_p - Q/2$ for the calculation of the (p, n) form factor (4) and OP in the outgoing channel (9). In all cases, the isovector nucleon OP given by the best-fit parameters agree closely with the JLM results in the same way as shown in Figs. 4 and 5 for $E = 35$ and 45 MeV. The numerical parameters of isovector density dependence (20) at different energies E can be obtained from the authors upon request. For the HF calculation of nuclear matter, the isovector density dependence (20) of the CDM3Y6 interaction at energy E approaching zero has also been constructed based on the JLM results [39] for low energies ($0 < E < 10$ MeV). This set of density dependent parameters is used in the present work to calculate the density dependent NM symmetry energy $S(\rho)$, defined in Eq. (2), by the HF method developed in Ref. [12] explicitly for use with the isospin- and density dependent M3Y interaction.

In the context of a fully microscopic OP, it is also desirable to have a realistic *imaginary* isoscalar density dependence for use in the folding calculation with the real isoscalar density dependence (16) of the CDM3Y6 interaction. Thus, we define the imaginary isoscalar interaction based on the same density dependent functional (20) as

$$w_{00}^{\text{D(EX)}}(E, \rho, s) = F_{\text{IS}}^{\text{W}}(E, \rho) v_{00}^{\text{D(EX)}}(s), \quad (25)$$

then the imaginary isoscalar nucleon OP in the nuclear limit is given by

$$W_{\text{IS}}(E, \rho) = F_{\text{IS}}^{\text{W}}(E, \rho) \{ \rho J_{00}^{\text{D}} + \int [\rho_n \hat{j}_1(k_F^n r) + \rho_p \hat{j}_1(k_F^p r)] v_{01}^{\text{EX}}(r) j_0(kr) d^3r \}. \quad (26)$$

Here $J_{00}^{\text{D}} = \int v_{00}^{\text{D}}(r) d^3r$, and other involved variables are determined in the same way as those in Eq. (23). In a similar manner, the parameters of $F_{\text{IS}}^{\text{W}}(E, \rho)$ have been searched at each energy to reproduce the JLM results tabulated in Ref. [28]. As an example, the isoscalar potential $W_{\text{IS}}(E, \rho)$ given by the best-fit parameters and the corresponding JLM

potential at $E = 35$ and 45 MeV are shown in Fig. 6. We must note that the imaginary OP

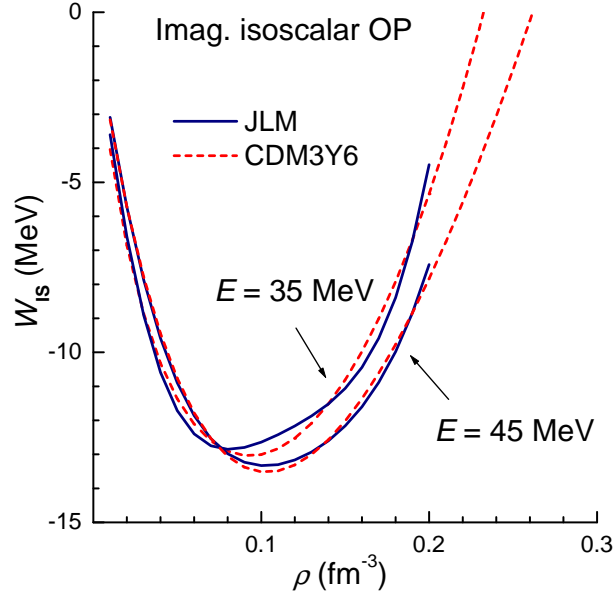


FIG. 6: (Color online) imaginary part $W_{\text{IS}}(E, \rho)$ of the isoscalar nucleon OP given by the isoscalar density dependent interaction (25) in comparison with the JLM results [28] at $E = 35$ and 45 MeV.

based on the JLM results for nuclear matter describes the absorption due to the Pauli blocking effect which leads to a *finite* mean-free path of nucleons in nuclear medium. As a result, $W_{\text{IS}}(E, \rho)$ tends to have a volume shape (deep in the center and shallow at the surface). In general, the imaginary nucleon OP at low and medium energies has been found [7, 8] to be best represented by a combination of volume and surface terms. The surface absorption is caused mainly by the collective excitations and transfer reactions which occur in the nuclear surface and are not related to the “volume” absorption given by $W_{\text{IS}}(E, \rho)$.

In conclusion, we have used the HF method (23)-(26) to construct a complex isovector density dependence of the CDM3Y6 interaction based on the JLM results for the nucleon OP in nuclear matter [28]. In connection with our study, we recall that the original version of the JLM interaction was simply deduced from the JLM nucleon OP in nuclear matter using a local density approximation and smeared out in the coordinate space by a single Gaussian [28, 44]. For example, the real part of the original JLM interaction was constructed by this method from the real nucleon OP in nuclear matter $V_{\text{IS(IV)}}^{\text{JLM}}(E, \rho)$ as

$$v_{00(01)}(E, \rho, s) \sim \frac{V_{\text{IS(IV)}}^{\text{JLM}}(E, \rho)}{\rho} \exp\left(-\frac{s^2}{t^2}\right), \quad (27)$$

with the Gaussian range t chosen to give a good global fit to the elastic data. Since $V_{\text{IS(IV)}}^{\text{JLM}}(E, \rho)$ already contains strengths of both direct and exchange parts of the G-matrix, the nucleon-nucleus OP for finite nuclei is given by the direct folding integration (13) only. Despite the simplicity, the original JLM interaction has been used quite successfully to study the elastic nucleon-nucleus scattering [44] as well as the (p, n) reaction to IAS [45, 46].

B. Results and discussions

Given the new complex density dependence of CDM3Y6 interaction, the isoscalar and isovector parts of the nucleon-nucleus OP can be calculated explicitly by the single-folding approach (13)-(14). It is natural, as the first step, to check the OM description of elastic nucleon-nucleus scattering at the nearby energies using the complex microscopic OP

$$U(R) = N_V[V_{\text{IS}}(R) \pm V_{\text{IV}}(R)] + iN_W[W_{\text{IS}}(R) \pm W_{\text{IV}}(R)], \quad (28)$$

where the (+) sign pertains to incident neutron and (-) sign to incident proton. Note that the imaginary part $W_{\text{IS(IV)}}(R)$ of the OP is given by the same folding procedure (13)-(14) but using the imaginary parts (22) and (25) of the CDM3Y6 interaction constructed separately at each energy. U is further added by the spin-orbital potential (and proton-nucleus OP added also by the Coulomb potential) taken, for simplicity, from the CH89 systematics [7]. The strengths $N_{V(W)}$ of the complex folded OP are adjusted to the best OM fit to the elastic scattering data. The OM results obtained for the elastic proton scattering at 40 MeV on the targets under study are shown in Fig. 7. A good description of the measured elastic proton scattering data [40, 41] can be reached after the complex folded potential is renormalized by $N_V \approx 0.90 - 0.94$ and $N_W \approx 0.6 - 0.8$. The OM results obtained for the elastic neutron scattering are shown in Fig. 8 where the best-fit $N_V \approx 0.9$ and $N_W \approx 0.6 - 0.7$. To have accurate distorted waves for the CC study of $A_{\text{g.s.}}(p, n)\tilde{A}_{\text{IAS}}$ reaction, we have also tried a hybrid choice for the complex OP with its real part given by the folding model and imaginary part by a Woods-Saxon (WS) potential based on the CH89 global systematics [7]

$$U(R) = N_V[V_{\text{IS}}(R) \pm V_{\text{IV}}(R)] - i[W_v f(R) - 4a_w W_s \frac{df(R)}{dR}],$$

where $f(R) = 1/\{1 + \exp[(R - R_w)/a_w]\}$. (29)

The normalization factor N_V of the real folded potential as well as strengths of the volume (W_v) and surface (W_s) terms of the absorptive WS potential are fine tuned in each case to

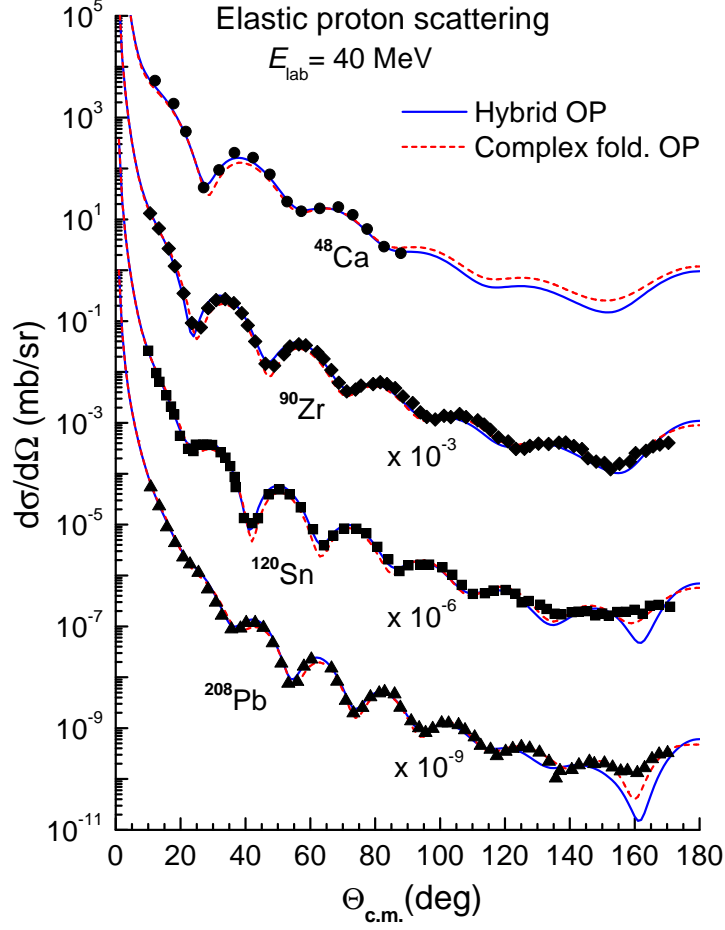


FIG. 7: (Color online) OM description of the elastic proton scattering from ^{48}Ca , ^{90}Zr , ^{120}Sn , and ^{208}Pb targets at 40 MeV obtained with the complex folded OP (28) and hybrid OP (29). The data were taken from Refs. [40, 41].

fit the elastic scattering data under study and/or reproduce in the OM calculation the total reaction cross section σ_R measured for the considered proton-nucleus systems at 35 and 45 MeV [43]. The OM descriptions of the elastic proton and neutron scattering given by such a hybrid choice for the nucleon OP are shown in Figs. 7 and 8 as solid curves. One can see that the OM fit given by the hybrid OP is slightly improved, especially, at forward scattering angles. Although the difference in the OM description of elastic nucleon scattering by the two choices of OP is marginal as seen in Figs. 7 and 8, their effect on the calculated (p, n) cross section is surprisingly much more significant.

After the OP for the entrance proton-nucleus channel is determined based on the OM

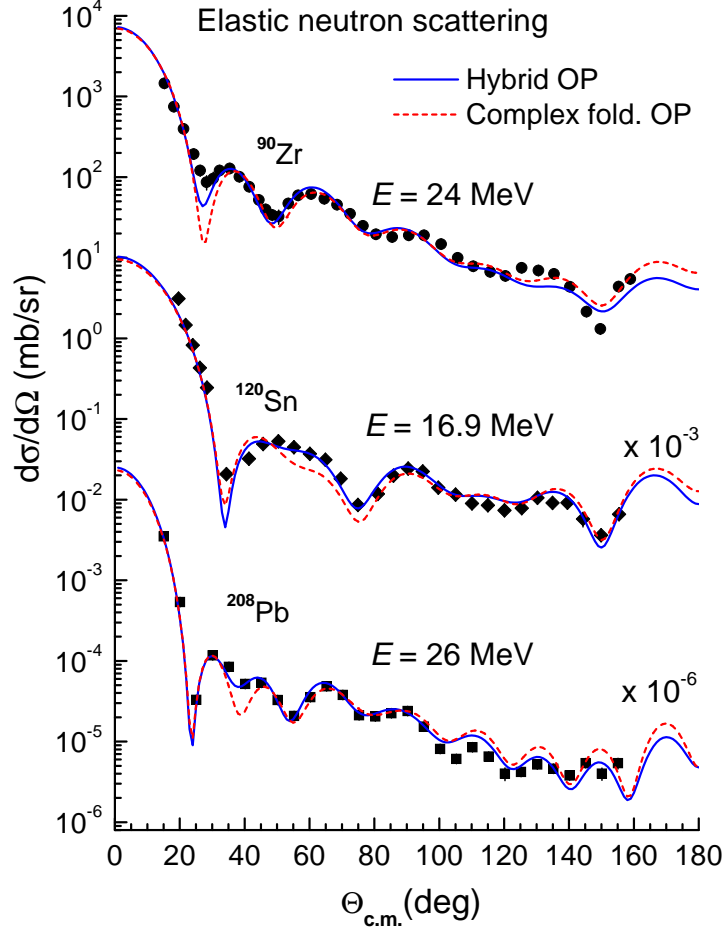


FIG. 8: (Color online) OM description of the elastic neutron scattering from ^{90}Zr , ^{120}Sn , and ^{208}Pb targets at energies of 17 to 24 MeV obtained with the complex folded OP and (28) and hybrid OP (29). The data were taken from Refs. [47, 48, 49].

analysis of the proton elastic scattering at the nearby energies, the (complex) charge exchange FF for the (p, n) transition channel is determined from the real and imaginary parts of the folded isovector potential (14), evaluated at $E = E_{\text{lab}} - Q/2$, as

$$F_{pn}(R) = \frac{2}{A} \sqrt{2T_z} U_1(R) = \sqrt{\frac{2}{T_z}} [N_R V_{\text{IV}}(R) + i N_I W_{\text{IV}}(R)]. \quad (30)$$

Keeping the OP parameters unchanged as fixed from the OM calculation described above, the normalization factors $N_{\text{R(I)}}$ of the folded charge exchange FF were adjusted for the best fit of the calculated (p, n) cross section to the data. In this way, the folding model analysis of the (p, n) reaction can serve as a good probe of the isospin dependence of the effective NN interaction. Since the elastic neutron scattering on a target being in its *excited* IAS cannot

be measured, the complex OP for the outgoing $n + \tilde{A}$ channel has been determined from the complex proton OP evaluated at the effective incident energy $E = E_{\text{lab}} - Q/2$, based on the isospin coupling (9). For consistency, the complex folded OP in the $n + \tilde{A}$ channel is renormalized by the same factors $N_{V(W)}$ as those used in entrance proton-nucleus channel. The WS imaginary part of the hybrid OP (29) in the outgoing $n + \tilde{A}$ channel is determined from the CH89 global OP using the same isospin coupling (9). The OP parameters used in our CC calculation of the (p, n) reaction are given in Tables II and III for the complex folded and hybrid OP, respectively.

We discuss now in details the CC results for the (p, n) reaction measured with ^{48}Ca target. The OM descriptions of the elastic $p + ^{48}\text{Ca}$ scattering data at 35 MeV [40] given by the complex folded OP (28), hybrid OP (29) and CH89 global OP [7] are shown in lower part of Fig. 9. Similar to the results at 40 MeV shown in Fig. 7, both complex folded and hybrid OP give a reasonable description of the measurement after their strengths were adjusted by the OM fit to the elastic data, with the complex folded OP slightly underestimating data at the forward angles. The CH89 global OP [7] sizably underestimates the elastic scattering data, and this is caused by a stronger absorption given by the CH89 imaginary OP. The CC descriptions of the $^{48}\text{Ca}_{\text{g.s.}}(p, n)^{48}\text{Sc}_{\text{IAS}}$ data at 35 MeV [11] given by the unrenormalized folded form factor (30) and that deduced from the isovector term of the CH89 potential using Eq. (4) are shown in upper part of Fig. 9, where the same OP's as those used in the lower part of Fig. 9 were taken for the entrance channel and the corresponding U_n potentials evaluated at $E = E_{\text{lab}} - Q/2$ taken for the outgoing channel. One can see that the unrenormalized folded FF gives a reasonable description of the measured (p, n) cross section at large angles while underestimates the data points at the forward angles. From the two choices of the OP, the complex folded OP (28) gives a worse fit to the (p, n) data at forward angles. Since the angular distribution at forward angles is more affected by the surface part of the OP and given the same real folded OP used in both calculations, the difference caused by the two OP's should be due to different surface absorptions described by the two OP's. The role of absorption is also seen in the CC description of the (p, n) data by the Lane FF determined from the CH89 parameters (denoted hereafter as CH89 form factor). Namely, the CH89 form factor sizably underestimates the data over the whole angular range when the OP's in the entrance and outgoing channels are taken exactly as given by the CH89 systematics [7]. The CC description by the CH89 form factor improves significantly when the best-fit hybrid

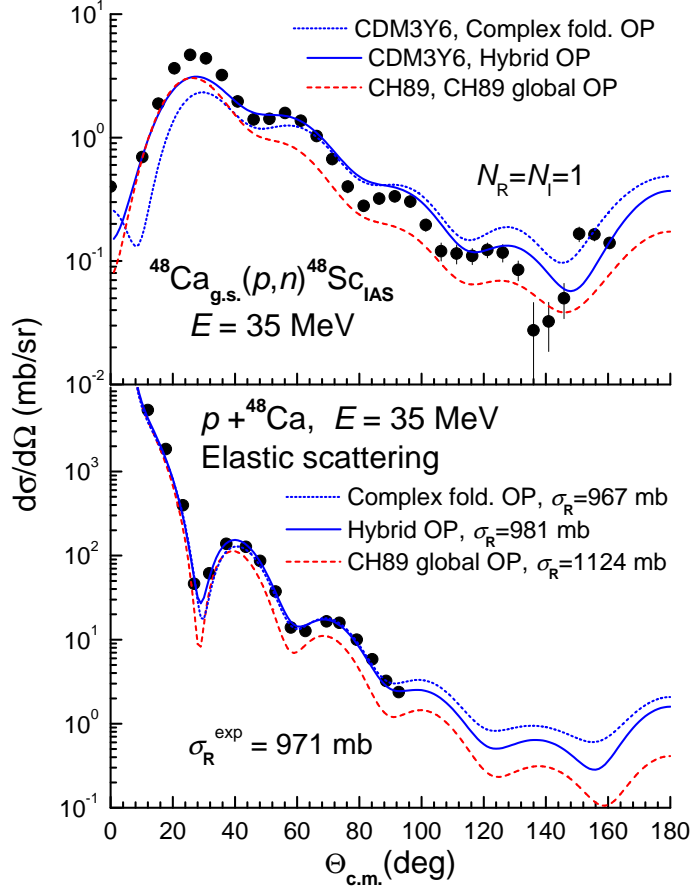


FIG. 9: (Color online) upper part: CC description of the $^{48}\text{Ca}_{g.s.}(p,n)^{48}\text{Sc}_{IAS}$ reaction at 35 MeV [11] given by the (unrenormalized) folded (p,n) form factor (30) and that deduced from Eq. (4) using the CH89 parameters [7]. Lower part: OM description of the elastic $p + ^{48}\text{Ca}$ scattering at 35 MeV [40] given by the complex folded OP (28), hybrid OP (29) and CH89 global OP [7].

OP (29) is used (see Fig. 10). Therefore, the unsatisfactory description of the (p,n) data by the CH89 form factor shown in upper part of Fig. 9 is caused by a too absorptive imaginary CH89 potential (which gives $\sigma_R \approx 1124$ mb compared to the measurement $\sigma_R^{\text{exp}} \approx 971 \pm 32$ mb [43]). We have further adjusted the complex strength of the folded FF to the best χ^2 -fit of the (p,n) data at 35 MeV [11], and N_R turns out to be around 1.3, while N_I remains close to unity (see lower part of Fig. 10 and Tables II and III). The deficiency of the complex folded OP cannot be eliminated by such an adjustment of the folded FF. A consistency check has also been made with all the folding and CC calculations redone using the real isovector component of CDM3Y6 interaction increased by a factor of 1.3, and all the calculated cross

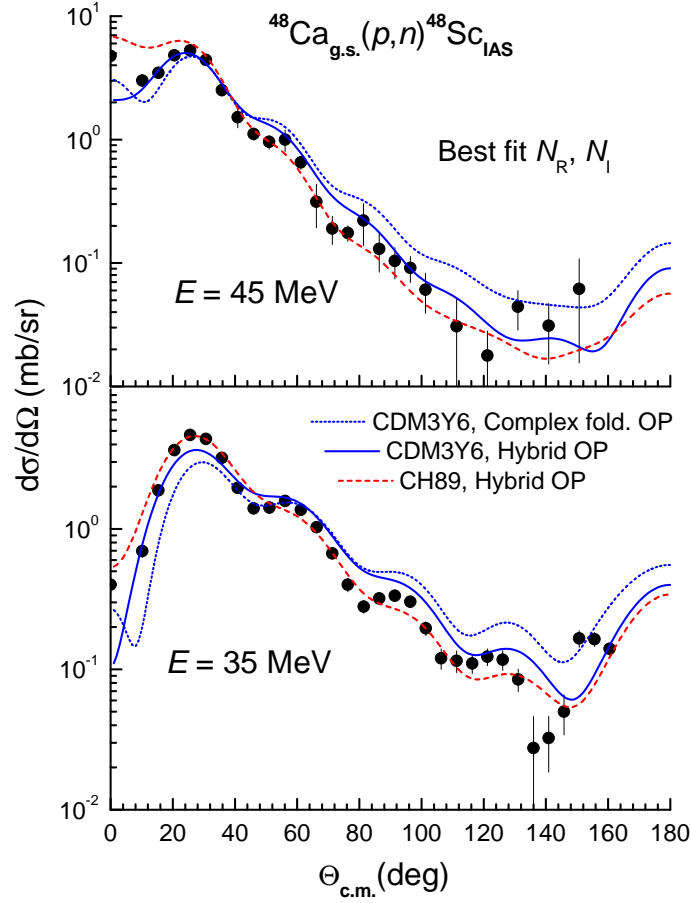


FIG. 10: (Color online) CC description of the $^{48}\text{Ca}_{\text{g.s.}}(p,n)^{48}\text{Sc}_{\text{IAS}}$ reaction [11] at 35 MeV (lower part) and 45 MeV (upper part) given by the renormalized folded (p,n) form factor (30) and that deduced from Eq. (4) using CH89 global OP [7], using two choices (28)-(29) of the OP.

sections remain about the same (as seen in the logarithmic graphing). The effect by the imaginary OP becomes more substantial in the CC analysis of the (p,n) data at 45 MeV (upper part of Fig. 10). While the use of the hybrid OP (29) results on about the same best-fit $N_{\text{R(I)}}$ coefficients of the folded FF as those found at 35 MeV, the complex folded OP (28) gives a much larger N_{R} of around 1.7 and a worse description of the (p,n) data at large angles. Since the real OP and complex folded FF are exactly the same in both calculations, the difference in the calculated (p,n) cross sections (solid and dotted lines in Fig. 10) is entirely due to the difference in the imaginary OP's. For illustration, we have plotted radial shapes of the $p+^{48}\text{Ca}$ optical potential at 45 MeV in Fig. 11. One can see that the real folded potential (renormalized by $N_{\text{V}} \approx 0.9$) is quite close in strength and

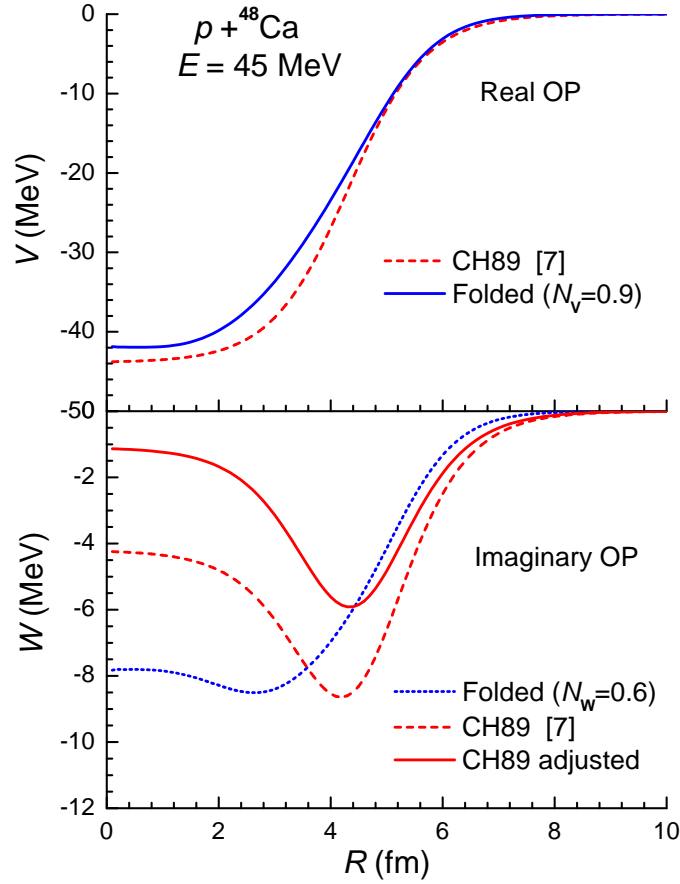


FIG. 11: (Color online) the real and imaginary parts of the complex folded OP (28) for $p+^{48}\text{Ca}$ system at 45 MeV, scaled by factors $N_{V(W)}$ given by the OM fit of the elastic data at 40 MeV, in comparison with the CH89 global OP taken from Ref. [7]. The adjusted imaginary CH89 potential has been used in the hybrid choice (29) of the OP.

shape to the global CH89 real OP. The situation with the imaginary OP is quite different: while the imaginary folded potential has a volume shape, the imaginary CH89 potential is strongly surface peaked even after its strengths W_v and W_s were reduced by the OM fit to the elastic proton scattering data. The obvious reason is that the imaginary folded potential (28) has been constructed based on the imaginary nucleon OP given by the BHF calculation of NM and is, therefore, of a “volume” nature. As a result, the imaginary folded potential cannot properly account for the surface absorption caused by inelastic scattering to the low-lying collective excitations and transfer reactions. The renormalization factor of the folded FF was driven to the excessive value of $N_R \approx 1.7$ by the use of the imaginary folded

TABLE II: Renormalization coefficients $N_{V(W)}$ of the complex folded proton-nucleus OP (28) used in the entrance channel. The calculated proton total reaction cross section σ_R is compared with the data σ_R^{exp} taken from Ref. [43]. $N_{R(I)}$ are the renormalization coefficients of the folded FF (30) deduced from the CC fit to the (p, n) data using the OP (28).

Target A	E (MeV)	N_V	N_W	σ_R (mb)	σ_R^{exp} (mb)	N_R	N_I
^{48}Ca	35	0.933	0.600	969	971 ± 32	1.356	0.970
	45	0.902	0.630	893	908 ± 34	1.738	1.054
^{90}Zr	35	0.893	0.731	1341	1316 ± 65^a	2.133	0.978
	45	0.893	0.731	1296	1214 ± 59^b	2.193	1.043
^{120}Sn	35	0.937	0.828	1605	1668 ± 59	2.372	0.981
	45	0.937	0.731	1588	1545 ± 38	2.529	0.985
^{208}Pb	35	0.916	0.747	1877	1974 ± 38	2.896	1.018
	45	0.916	0.747	1963	1979 ± 41	2.606	0.985

^a Total $p+^{90}\text{Zr}$ reaction cross section measured at $E = 40$ MeV; ^b at $E = 49.5$ MeV.

potential and *not* by the weakness of the isovector interaction (21) - (22). We note further that this subtle “absorption” effect has been established only in the CC calculation of the (p, n) reaction to IAS because the elastic nucleon scattering data at the nearby energies are still reasonably reproduced with the imaginary folded potential (see Figs. 7 and 8). Thus, the distorted waves χ_{pA} and $\chi_{n\bar{A}}$ given by the realistic hybrid OP (29) should be more accurate for the probe of the isovector density dependence in the CC analysis of the (p, n) reaction. The CC calculations using the hybrid OP (29) give a good overall description of the $^{48}\text{Ca}_{\text{g.s.}}(p, n)^{48}\text{Sc}_{\text{IAS}}$ data at 35 and 45 MeV with the folded FF renormalized by $N_R \approx 1.3$ and $N_I \approx 1$. These calculations also give the total (p, n) cross section $\sigma_{pn} \approx 10.7$ and 9.0 mb for the $^{48}\text{Ca}_{\text{g.s.}}(p, n)^{48}\text{Sc}_{\text{IAS}}$ reaction at 35 and 45 MeV, respectively, which agree well with the measured values [11], $\sigma_{pn}^{\text{exp}} \approx 10.2 \pm 1.1$ and 8.4 ± 1.0 mb at 35 and 45 MeV, respectively.

The results of our folding model analysis of the $^{90}\text{Zr}_{\text{g.s.}}(p, n)^{90}\text{Nb}_{\text{IAS}}$ reaction at the same energies are compared with the data in Fig. 12. One can see that the peak of the (p, n) cross section is weaker and only around half of that measured for $^{48}\text{Ca}_{\text{g.s.}}(p, n)^{48}\text{Sc}_{\text{IAS}}$ reaction.

TABLE III: Parameters of the hybrid OP (29) used in the entrance and exit channels. Parameters given in boldface were kept unchanged as determined from the CH89 systematics [7]. The calculated proton total reaction cross section σ_R is compared with the data σ_R^{exp} taken from Ref. [43]. $N_{R(I)}$ are the renormalization coefficients of the folded FF (30) deduced from the CC fit to the (p, n) data using the OP (29).

Target A	E (MeV)	Channel	N_V	W_v (MeV)	W_s (MeV)	R_w (fm)	a_w (fm)	σ_R (mb)	σ_R^{exp} (mb)	N_R	N_I
^{48}Ca	35	$p + A$	0.925	1.495	5.432	4.414	0.69	981	971 ± 32	1.265	0.960
		$n + \tilde{A}$	0.925	1.495	4.503	4.414	0.69	-	-	-	-
	45	$p + A$	0.900	1.096	5.358	4.414	0.69	893	908 ± 34	1.279	0.970
		$n + \tilde{A}$	0.900	1.096	3.985	4.414	0.69	-	-	-	-
^{90}Zr	35	$p + A$	0.913	1.479	6.060	5.540	0.69	1330	1316 ± 65^a	1.202	0.969
		$n + \tilde{A}$	0.913	1.891	5.267	5.540	0.69	-	-	-	-
	45	$p + A$	0.913	2.434	5.314	5.540	0.69	1296	1214 ± 59^b	1.298	1.081
		$n + \tilde{A}$	0.913	2.918	4.721	5.540	0.69	-	-	-	-
^{120}Sn	35	$p + A$	0.937	2.305	7.792	6.140	0.69	1637	1668 ± 59	1.203	0.950
		$n + \tilde{A}$	0.937	1.686	4.687	6.140	0.69	-	-	-	-
	45	$p + A$	0.937	2.027	6.529	6.140	0.69	1570	1545 ± 38	1.225	0.958
		$n + \tilde{A}$	0.937	2.653	4.218	6.140	0.69	-	-	-	-
^{208}Pb	35	$p + A$	0.901	2.419	8.729	7.460	0.69	1964	1974 ± 38	1.201	0.955
		$n + \tilde{A}$	0.901	1.127	4.386	7.460	0.69	-	-	-	-
	45	$p + A$	0.901	2.827	6.334	7.460	0.69	1998	1979 ± 41	1.150	0.930
		$n + \tilde{A}$	0.901	1.871	4.000	7.460	0.69	-	-	-	-

^a Total $p+^{90}\text{Zr}$ reaction cross section measured at $E = 40$ MeV; ^b at $E = 49.5$ MeV.

A weaker charge exchange strength also results on the total (p, n) cross section of about 50% smaller than that obtained for ^{48}Ca target (see Table I in Ref. [11]). In terms of the isospin-flip transition (4), the charge exchange (p, n) strength is directly proportional to the neutron-proton asymmetry parameter $\delta = (N - Z)/A$ and strength of the Lane potential U_1 . Indeed, the isovector folded potential $V_{IV}(R)$ for the $p+^{48}\text{Ca}$ system is about 30-40% larger than that obtained for the $p+^{90}\text{Zr}$ system at the surface distances and the asymmetry

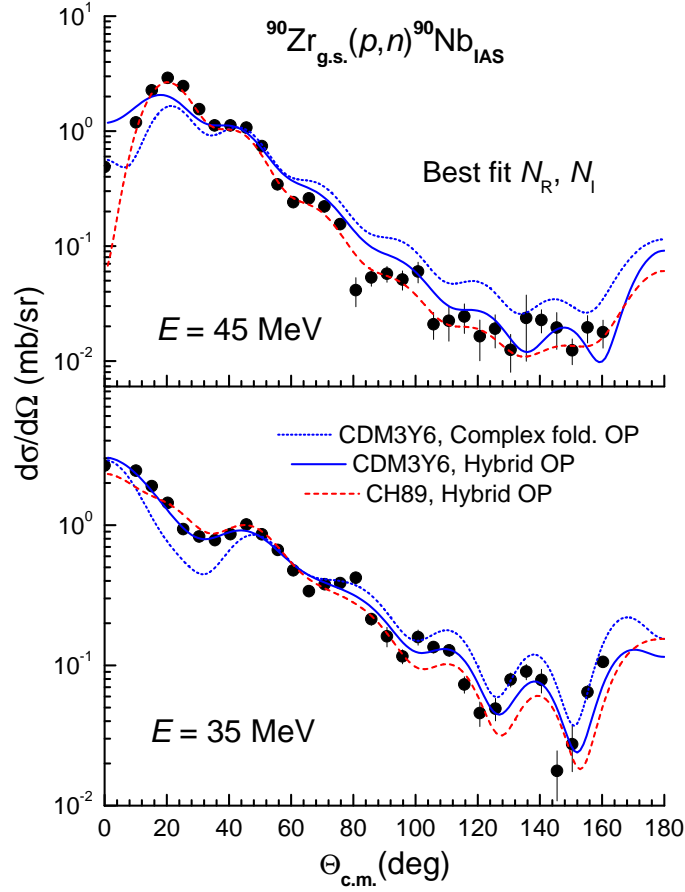


FIG. 12: (Color online) the same as Fig. 10 but for the $^{90}\text{Zr}_{\text{g.s.}}(p, n)^{90}\text{Nb}_{\text{IAS}}$ reaction [11].

parameter $\delta \approx 0.17$ and 0.11 for ^{48}Ca and ^{90}Zr , respectively. A weaker charge exchange strength observed in the $^{90}\text{Zr}_{\text{g.s.}}(p, n)^{90}\text{Nb}_{\text{IAS}}$ reaction is, therefore, well anticipated. Like the $p+^{48}\text{Ca}$ system, the use of the complex folded OP (28) in the CC calculation with the folded FF gives a poor description of the (p, n) data, especially at forward angles (see Fig. 12), even after its real strength is renormalized by $N_R > 2$ as determined from the χ^2 fit to the data. A strongly “volume” imaginary folded potential is also the reason for this disagreement. The same folded FF gives a much better fit to the (p, n) data when the hybrid OP (29) is used and its complex strengths need to be renormalized by just $N_R \approx 1.2 - 1.3$ and $N_I \approx 1$ which are close to those obtained for the $p+^{48}\text{Ca}$ system (see Table III). The CH89 form factor for the $p+^{90}\text{Zr}$ system slightly underestimates the data if the OP in the entrance and exit channels are determined as given by the CH89 parameters. However, the CC description of the (p, n) data by the CH89 form factor is much better when the hybrid

OP (29) is used. The CC calculation using the hybrid OP and renormalized folded FF gives the total (p, n) cross section $\sigma_{pn} = 4.8$ and 4.1 mb for the $^{90}\text{Zr}_{\text{g.s.}}(p, n)^{90}\text{Nb}_{\text{IAS}}$ reaction at 35 and 45 MeV, respectively, which agree nicely with the data ($\sigma_{pn}^{\text{exp}} \approx 4.8 \pm 0.5$ and 4.4 ± 0.5 mb at 35 MeV and 45 MeV, respectively) [11].

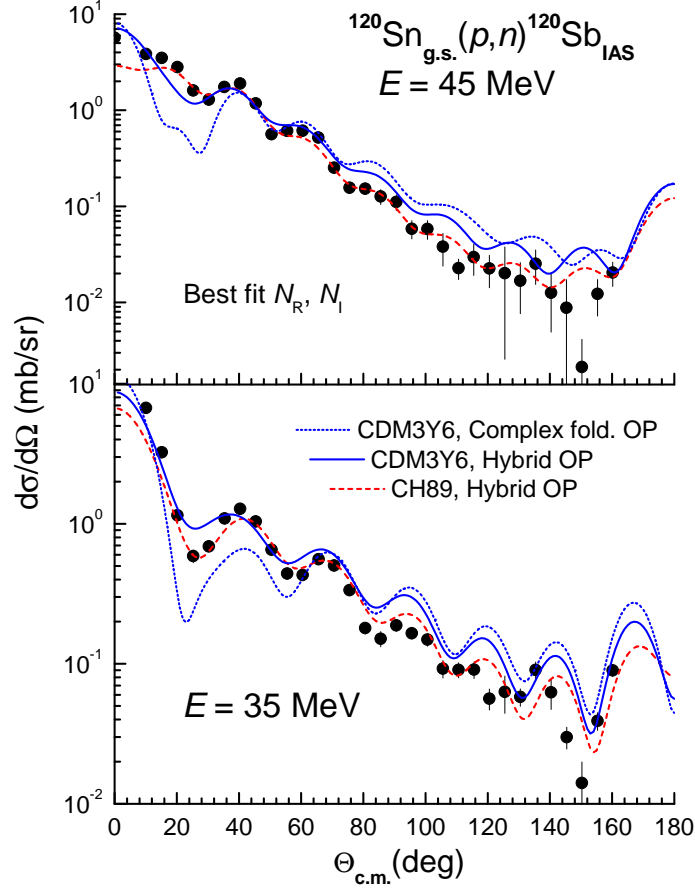


FIG. 13: (Color online) the same as Fig. 10 but for the $^{120}\text{Sn}_{\text{g.s.}}(p, n)^{120}\text{Sb}_{\text{IAS}}$ reaction [11].

The CC results for the $^{120}\text{Sn}_{\text{g.s.}}(p, n)^{120}\text{Sb}_{\text{IAS}}$ and $^{208}\text{Pb}_{\text{g.s.}}(p, n)^{208}\text{Bi}_{\text{IAS}}$ reactions are presented in Figs. 13 and 14, respectively. Like the results obtained above for ^{48}Ca and ^{90}Zr targets, the use of the complex folded OP (28) with a volume-shape imaginary part leads to a wrong shape of the calculated (p, n) cross section at forward angles (see, in particular, Fig. 13). The CC description of the (p, n) data by both the folded FF and CH89 form factors is very satisfactory when the hybrid OP's (which describe well the proton elastic scattering at 40 MeV and measured total reaction cross section) are used for the entrance and exit channels. A stronger proton-nucleus Coulomb potential seems to push the main peak of the

(p, n) cross section to the forward angles (compare, e.g., Figs. 10 and 14), but the measured data points in the observable angular range still allow us to make an accurate conclusion on the complex strength of the folded (p, n) form factor (30). For the two heavy targets, the best CC fit by the folded FF is reached when its real and imaginary strengths are scaled by $N_R \approx 1.2$ and $N_I \approx 1$ which are reasonably close to those obtained for ^{48}Ca and ^{90}Zr targets. Although the complex folded OP (28) can be used to reasonably describe the elastic

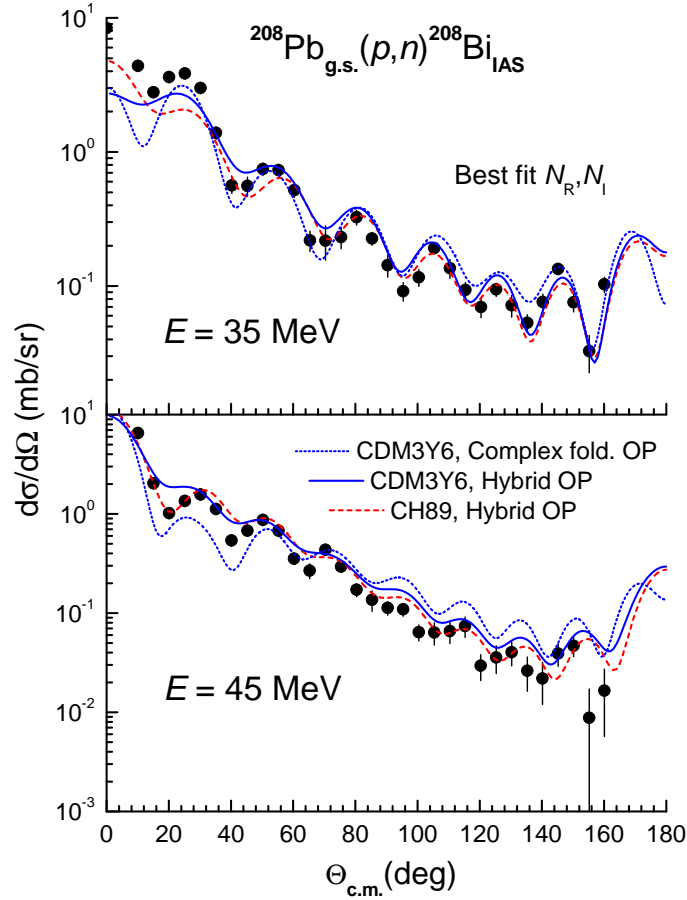


FIG. 14: (Color online) the same as Fig. 10 but for the $^{208}\text{Pb}_{\text{g.s.}}(p, n)^{208}\text{Bi}_{\text{IAS}}$ reaction [11].

proton and neutron scattering on the targets under study, the volume absorption given by its imaginary part strongly affects the distorted waves χ_{pA} and $\chi_{n\bar{A}}$ at the surface and, hence, leads to a poor description of the (p, n) data at forward angles and a much stronger renormalization of the folded FF. In general, a fully Lane consistent and accurate description of both the nucleon elastic scattering and (p, n) reaction to IAS should be reached with a more accurate microscopic model for the imaginary OP, like that developed for the nucleon OP

at low energies [50], capable to take into account explicitly coupling to the most collective particle-hole excitations in the target which lead to the surface absorption. Given such a strong impact by the absorption to the calculated (p, n) cross section, the renormalization factors of the folded (p, n) form factor $N_{R(I)}$ obtained with the complex folded OP should not be considered as due to the weakness of the isovector density dependence of the CDM3Y6 interaction. We must, therefore, rely on the best-fit $N_{R(I)}$ coefficients obtained with the hybrid OP (29) in deducing the strength of the isovector density dependence. Our present results emphasize that an accurate determination of the imaginary nucleon-nucleus OP is very important, especially, in the DWBA or CC studies of direct reactions measured with unstable nuclei when elastic scattering data are not always available.

In connection with the present study, we note that the original version of the effective JLM interaction (27) has been used by Pakou *et al.* [45] and Bauge *et al.* [46] to study the same (p, n) reactions. The JLM folding-model analysis of the proton, neutron elastic scattering and (p, n) charge exchange reaction done in Ref. [45] has also shown that the isovector part of the JLM interaction is too weak and a very strong overall renormalization of the folded FF by $N_R = N_I \approx 2 - 2.5$ is needed to account for the measured (p, n) cross sections. In view of our results obtained with the complex folded OP (28), it is very likely that such large renormalization of the folded FF has been driven by the “volume” absorption of the JLM complex OP used in Ref. [45]. In a more elaborate treatment of the charge exchange transition within the JLM model, Bauge *et al.* [46] have made the isospin coupling factor in Eq. (4) density dependent, i.e., $\sqrt{2T_z/A} = \sqrt{[\rho_n(r) - \rho_p(r)]/\rho(r)}$, and included it into the (direct) folding integral. The JLM nucleon OP obtained in such a density-dependent isospin coupling assumption has been thoroughly tested in the OM analysis of the proton, neutron elastic scattering and (p, n) reaction over a wide range of energies and target masses, and one can deduce from the results shown in Fig. 1 of Ref. [46] the best-fit renormalization coefficients of the (p, n) folded form factor $N_R \approx 1.5 - 1.6$ and $N_I \approx 1.3 - 1.4$, in the energy range of 30 – 40 MeV, which are closer to our results. Despite differences in the best-fit renormalization coefficients of the folded FF obtained in the present work and in the JLM folding-model analyses [45, 46], all the results show consistently that the isovector strength of the JLM interaction is much too weak to account for the measured (p, n) data. Since the isovector term of the JLM nucleon OP has been obtained as the first-order expansion of the mass operator of symmetric nuclear matter perturbed by a neutron excess [51], a

weakness of the resulting JLM nucleon OP in asymmetric NM could well be expected. As the charge exchange reaction to IAS is quite helpful in probing the isospin dependence of the effective NN interaction, it would be of interest to apply similar folding model analysis to test the isospin dependence of the nucleon OP given by more advanced BHF calculations of asymmetric NM, like that by Zuo *et al.* [29].

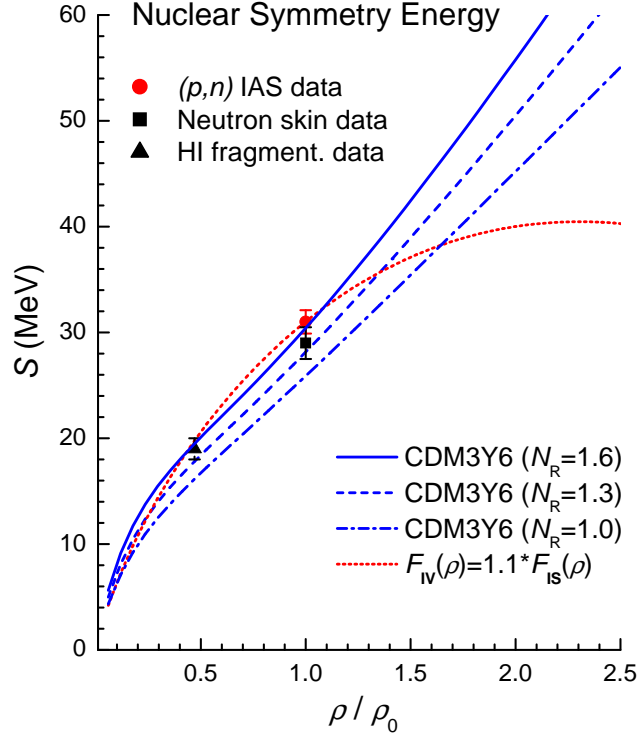


FIG. 15: (Color online) density dependence of the nuclear symmetry energy $S(\rho)$ given by the HF calculation of asymmetric NM [12] using different isovector density dependences of the CDM3Y6 interaction and the empirical values deduced from the CC analysis of the $p(^6\text{He}, ^6\text{Li}^*)n$ reaction [26] as well as the neutron-skin [21] and HI fragmentation [23, 24] studies. See more discussion in the text.

As mentioned above, the knowledge about the isospin dependence of the in-medium NN interaction is of vital importance in studying the equation of state of asymmetric NM, the key input for the understanding of the dynamics of supernova explosion and neutron star formation [14, 15, 16]. We show here that the folding model analysis of the (p, n) reaction can be quite helpful for the determination of the nuclear symmetry energy. After the real

isovector density dependence (20) of the CDM3Y6 interaction at energy approaching zero has been carefully parameterized on the HF level to match the microscopic BHF results [39], the density- and isospin dependent CDM3Y6 interaction is further used to calculate the nuclear symmetry energy $S(\rho)$ using the standard HF method [12] and the results are shown in Fig. 15. One can see that $E_{\text{sym}} = S(\rho_0)$ is lying somewhat lower than the empirical value of around 30 – 31 MeV if $F_{\text{IV}}^{\text{V}}(\rho)$ is taken as determined from the BHF results by JLM [28]. The weakness of the JLM isovector interaction is, thus, also confirmed in our HF calculation of asymmetric NM. A very good agreement with the empirical E_{sym} values is reached when $F_{\text{IV}}^{\text{V}}(E \approx 0, \rho)$ is scaled by a factor $N_{\text{R}} \approx 1.3 - 1.6$, which is slightly larger than factor N_{R} for $F_{\text{IV}}^{\text{V}}(E, \rho)$ at $E = 35$ and 45 MeV deduced from our folding model analysis of the (p, n) reaction. The renormalized strength of the isovector density dependence also gives a good agreement with the empirical symmetry energy at the half-density point, $S(\rho \approx 0.08 \text{ fm}^{-3}) \approx 18 - 22 \text{ MeV}$, found from recent studies [23, 24] of the heavy-ion fragmentation in the same energy region as that considered in our study of (p, n) reactions. It should be noted that analysis of HI fragmentation data was made based on the antisymmetrized molecular dynamics simulations [23] which obtained $S(\rho \approx 0.08 \text{ fm}^{-3})$ at a *finite* temperature of around 3 MeV. Therefore, this value approximately agrees with our HF result for the low-density part of $S(\rho)$ shown in Fig. 15 only if the temperature dependence of $S(\rho)$ at low NM densities is neglected. Finally we note that our results are also complementary to the structure studies which relate the E_{sym} value to the neutron skin, a method first suggested by Brown [19]. If one adopts a neutron-skin $\Delta R \approx 0.1 - 0.2 \text{ fm}$ for ^{208}Pb then a systematics based on the mean-field calculations [21] gives $E_{\text{sym}} \approx 27 - 31 \text{ MeV}$ (which is plotted as solid square in Fig. 15). Although the folding model analysis of the (p, n) reaction has put a constraint on the nuclear symmetry energy $S(\rho)$ at $\rho \leq \rho_0$, its behavior at high densities remains unexplored in our study due to a simple reason that the total nuclear density of the proton-nucleus system never exceeds ρ_0 , so that the (p, n) reaction is sensitive to the low-density part of the isovector interaction only. In particular, when the isovector density dependence $F_{\text{IV}}(\rho)$ is taken to have the same functional form as the isoscalar density dependence $F_{\text{IS}}(\rho)$, and scaled by a factor of 1.1 deduced from our recent CC analysis of the $p(^6\text{He}, ^6\text{Li}^*)n$ data [26], it gives nearly the same description of the symmetry energy $S(\rho)$ at $\rho \leq \rho_0$ as the newly parameterized isovector density dependence (see dotted curve in Fig. 15). The two sets of the isovector density dependence have, however, very different behaviors at high NM densities.

The $S(\rho)$ curves obtained with the isovector density dependence based on the BHF results of asymmetric NM increase monotonically with the increasing NM density. Such a behavior has been recently discussed as the *asy-stiff* density dependence of the nuclear symmetry energy, while the $S(\rho)$ curve given by $F_{IV}(\rho)$ having the same functional form as $F_{IS}(\rho)$ can be referred to as the *asy-soft* density dependence (see more discussion in Ref. [52]). Although some HI collision data seem to prefer the stiff density dependence of the symmetry energy [52], much more studies need to be done before a definitive conclusion can be made. In particular, a double-folding approach to study the $(^3\text{He}, t)$ or $(^{13}\text{C}, ^{13}\text{N})$ reactions exciting IAS might allow us to test the high density part of the isovector density dependence (20), due to a higher overlap nuclear density reached during the collision and, eventually, to probe the nuclear symmetry energy $S(\rho)$ at higher NM densities.

V. SUMMARY

A consistent CC analysis of the charge exchange (p, n) reactions to the isobaric analog states of the ground states of ^{48}Ca , ^{90}Zr , ^{120}Sn and ^{208}Pb targets at the proton incident energies of 35 and 45 MeV has been done using the (p, n) form factors either calculated microscopically in the folding model [4] or determined from the empirical WS parameters of the existing nucleon global OP's [6, 7, 8].

Although the isospin dependence of the CH89 global OP [7] has been established based only on the OM studies of the elastic proton and neutron scattering only, it can be used to determine the charge exchange FF for the (p, n) transition to IAS, based the isospin coupling (4). This CH89 form factor was shown to account quite well for the (p, n) data if the parameters of the proton OP are fine tuned to reproduce the measured elastic proton scattering and total reaction cross sections σ_R .

To probe of the isospin dependence of the effective NN interaction, a complex isovector density dependence of the CDM3Y6 interaction [27] has been carefully parameterized based on the density dependent JLM nucleon OP [28] and used further in the folding model analysis of the (p, n) reaction. Like previous studies [45, 46] using the original JLM interaction (27), the present results also show that the isovector strength of the JLM interaction is quite weak to account for the observed (p, n) transitions. The CC results obtained with realistic (semi-microscopic) nucleon OP's for the entrance and exit channels have shown that the

real isovector density dependence needs to be enhanced by about 20 – 30% to give a good description of the (p, n) reaction.

The isovector density dependence of the CDM3Y6 interaction has also been constructed based on the JLM nucleon OP at energy approaching zero for further use in the HF study of asymmetric NM. The HF calculation using this new isovector interaction gives the nuclear symmetry energy $S(\rho)$ close to the empirical values at $\rho \leq \rho_0$ when the real isovector density dependence is scaled by a factor $N_R \approx 1.3 - 1.6$. This result confirms the weakness of the isovector strength of the JLM interaction found in the folding model analysis of the (p, n) reaction at 35 and 45 MeV. The new isovector density dependence predicts a behavior of $S(\rho)$ at high NM densities similar to what discussed recently in the literature [52] as the *asy-stiff* density dependence of the symmetry energy.

Acknowledgement

We thank A. Pakou for her helpful communication on the (p, n) reactions under study. This research project has been supported, in part, by the Natural Science Council of Vietnam, EU Asia-Link Program CN/Asia-Link/008 (94791) and Vietnam Atomic Energy Commission (VAEC).

-
- [1] G.R. Satchler, R.M. Drisko, and R.H. Bassel, Phys. Rev. **136**, B637 (1964).
 - [2] A.M. Lane, Phys. Rev. Lett. **8**, 171 (1962).
 - [3] G.R. Satchler, *Direct Nuclear Reactions* (Clarendon Press, Oxford, 1983).
 - [4] D.T. Khoa, E. Khan, G. Colò, and N. Van Giai, Nucl. Phys. **A706**, 61 (2002).
 - [5] D.T. Khoa, Phys. Rev. C **68**, 011601(R) (2003).
 - [6] F.D. Becheetti and G.W. Greenlees, Phys. Rev. **182**, 1190 (1969).
 - [7] R.L. Varner, W.J. Thompson, T.L. McAbee, E.J. Ludwig, and T.B. Clegg, Phys. Rep. **201**, 57 (1991).
 - [8] A.J. Koning and J.P. Delaroche, Nucl. Phys. **A713**, 231 (2003).
 - [9] J.D. Carlson, C.D. Zafiratos, and D.A. Lind, Nucl. Phys. **A249**, 29 (1975).
 - [10] G.C. Jon *et al.*, Phys. Rev. C **62**, 044609 (2000).

- [11] R.R. Doering, D.M. Patterson, and A. Galonsky, Phys. Rev. C **12**, 378 (1975).
- [12] D.T. Khoa, W. von Oertzen, and A.A. Ogloblin, Nucl. Phys. **A602**, 98 (1996).
- [13] W. Zuo, I. Bombaci, and U. Lombardo, Phys. Rev. C **60**, 024605 (1999).
- [14] H.A. Bethe, Rev. Mod. Phys. **62**, 801 (1990).
- [15] F.D. Swesty, J.M. Lattimer, and E.S. Myra, Astrophys. J. **425**, 195 (1994).
- [16] A.W. Steiner, M. Prakash, J.M. Lattimer, and P.J. Ellis, Phys. Rep. **411**, 325 (2005).
- [17] M. Brack, C. Guet, and H.B. Håkansson, Phys. Rep. **123**, 276 (1985).
- [18] J.M. Pearson and R.C. Nayak, Nucl. Phys. **A668**, 163 (2000).
- [19] B.A. Brown, Phys. Rev. Lett. **85**, 5296 (2000).
- [20] C.J. Horowitz and J. Piekarewicz, Phys. Rev. Lett. **86**, 5647 (2001).
- [21] R.J. Furnstahl, Nucl. Phys. **A706**, 85 (2002).
- [22] A.E.L. Dieperink, Y. Dewulf, D. Van Neck, M. Waroquier, and V. Rodin, Phys. Rev. C **68**, 064307 (2003).
- [23] A. Ono, P. Danielewicz, W.A. Friedman, W.G. Lynch, and M.B. Tsang, Phys. Rev. C **70**, 041604(R) (2004).
- [24] D.V. Shetty, S.J. Yennello, A.S. Botvina, G.A. Souliotis, M. Jandel, E. Bell, A. Keksis, S. Soisson, B. Stein, and J. Iglio, Phys. Rev. C **70**, 011601(R) (2004).
- [25] L.W. Chen, C.M. Ko, and B.A. Li, Phys. Rev. Lett. **94**, 032701 (2005).
- [26] D.T. Khoa and H.S. Than, Phys. Rev. C **71**, 044601 (2005).
- [27] D.T. Khoa, G.R. Satchler, and W. von Oertzen, Phys. Rev. C **56**, 954 (1997).
- [28] J.P. Jeukenne, A. Lejeune, and C. Mahaux, Phys. Rev. C **16**, 80 (1977).
- [29] W. Zuo, L.G. Cao, B.A. Li, U. Lombardo, and C.W. Shen, Phys. Rev. C **72**, 014005 (2005).
- [30] N. Anantaraman, H. Toki, and G.F. Bertsch, Nucl. Phys. **A398**, 269 (1983).
- [31] W.G. Love, Phys. Rev. C **15**, 1261 (1977).
- [32] D.T. Khoa and W. von Oertzen, Phys. Lett. **B342**, 6 (1995); D.T. Khoa *et al.* Phys. Rev. Lett. **74**, 34 (1995).
- [33] M. Grasso, N. Sandulescu, N. Van Giai, and R.J. Liotta, Phys. Rev. C **64**, 064321 (2001).
- [34] J. Raynal, Computing as a Language of Physics (IAEA, Vienna, 1972) p.75; J. Raynal, coupled-channel code ECIS97 (unpublished).
- [35] F.A. Brieva and J.R. Rook, Nucl. Phys. **A291**, 317 (1977).
- [36] J. Hüfner and C. Mahaux, Ann. Phys. **73**, 525 (1972).

- [37] D.T. Khoa and W. von Oertzen, Phys. Lett. **B304**, 8 (1993).
- [38] A.L. Fetter and J.D. Walecka, *Quantum Theory of Many-Particle Systems* (Dover Publications Inc., 2003).
- [39] A. Lejeune, Phys. Rev. C **21**, 1107 (1980).
- [40] C.R. Gruhn, T.Y.T. Kuo, C.J. Maggiore, and B.M. Preedom, Phys. Rev. C **6**, 944 (1972).
- [41] M.P. Fricke, E.E. Gross, B.J. Morton, and A. Zucker, Phys. Rev. **156**, 1207 (1967).
- [42] D.T. Khoa, W. von Oertzen, H.G. Bohlen, and S. Ohkubo, J. Phys. G **34**, R111 (2007).
- [43] R.F. Carlson, At. Data and Nucl. Data Tables **63**, 93 (1996).
- [44] E. Bauge, J.P. Delaroche, and M. Girod, Phys. Rev. C **58**, 1118 (1998).
- [45] A. Pakou, N. Alamanos, P. Roussel-Chomaz, F. Auger, D. Rosengrant, and A. de Vismes, Nucl. Phys. **A691**, 661 (2001).
- [46] E. Bauge, J.P. Delaroche, and M. Girod, Phys. Rev. C **63**, 024607 (2001).
- [47] Y. Wang and J. Rapaport, Nucl. Phys. **A517**, 301 (1990).
- [48] P.P. Guss, R.C. Byrd, C.R. Howell, R.S. Pedroni, G. Tungate, and R.L. Walter, Phys. Rev. C **39**, 405 (1989).
- [49] J. Rapaport, T.S. Cheema, D.E. Bainum, R.W. Finlay, and J. D. Carlson, Nucl. Phys. **A296**, 95 (1978).
- [50] C. Barbieri and B.K. Jennings, Phys. Rev. C **72**, 014613 (2005).
- [51] J.P. Jeukenne, A. Lejeune, and C. Mahaux, Phys. Rev. C **15**, 10 (1977).
- [52] V. Barana, M. Colonna, V. Greco, and M. Di Toro, Phys. Rep. **410**, 335 (2005).